Journal of Alloys and Compounds 775 (2019) 1213–1220

Contents lists available at ScienceDirect

Journal of Alloys and Compounds

journal homepage: http://www.elsevier.com/locate/jalcom

Improved performance of a back-illuminated GaN-based metal-semiconductor-metal ultraviolet photodetector by *in-situ* modification of one-dimensional ZnO nanorods on its screw dislocations

Y.P. Chen [a], C.H. Zheng [a, **], L.Q. Hu [b], Y.R. Chen [c, *]

[a] College of Resource and Environment, Quanzhou Normal University, Quanzhou 362000, People's Republic of China
[b] Institute of Optoelectronic Technology, Fuzhou University, Fuzhou 350002, People's Republic of China
[c] State Key Laboratory of Luminescence and Applications, Changchun Institute of Optics, Fine Mechanics and Physics, Chinese Academy of Sciences, Changchun 130033, People's Republic of China

ARTICLE INFO

Article history:
Received 2 August 2018
Received in revised form
18 October 2018
Accepted 22 October 2018
Available online 23 October 2018

Keywords:
GaN-based ultroviolet photodetectors
ZnO nanorods modification
Screw dislocation passivation
Photoelectric performance improvement
Metal-semiconductor-metal

ABSTRACT

It is a critical challenge to realize efficient GaN-based UV photodetectors (UV-PDs) due to the existence of high-density dislocations in the epilayers prepared by heteroepitaxy. In this paper, the method of *in-situ* modifying the screw dislocations in GaN-based materials with one-dimensional (1D) ZnO nanorods by screw dislocation-driven self-assembled solution growth is developed to engineer and improve the photoelectric performances of the back-illuminated metal-semiconductor-metal (MSM) structure p-GaN UV-PDs. The results show that the *in-situ* grown 1D ZnO nanorods on the dislocations plays the roles of passivating the dislocations to suppress the dark current, improving the spectral response intensity and extending the spectral response band of the MSM structure UV-PDs. The *in-situ* modification of 1D ZnO nanomaterials can be developed into a method to engineer and modify the defects viz. threading dislocations of the GaN-based semiconductors so as to achieve the purpose of regulating the performance of the related optoelectronic devices, which can be extended to other material systems of optoelectronic devices.

1. Introduction

The filter-free, full solid-state ultraviolet photodetectors (UV-PDs) have drawn a significant attention in military and civil fields for their potential applications in missile early warning, flame warning, UV radiation monitoring in the environment, biological agent detection, and so on [1–3]. As one of the third generation of semiconductors, the GaN-based materials which have achieved a great success in the fields of light-emitting diodes (LEDs) [4–7], laser diodes (LDs) [8,9], and high electron mobility transistors (HEMTs) [10,11] are attracting a growing concern over the UV-PDs because of their wide direct band gap, full solid-state, intrinsic cut-off, anti-radiation, and excellent chemical and thermal stability [12]. However, up to present, the performance of the GaN-based UV-PDs is still restricted by the high-density threading dislocations in GaN epilayers for the reason that the preparation of GaN is mainly performed on the heterogeneous substrates such as Al_2O_3, SiC and Si by the heteroepitaxy which remains the existing mainstream technique due to the lack of widely used homogeneous substrates. The high-density threading dislocations in a hetero-epitaxial grown GaN resulted from the large lattice and thermal expansion mismatch between GaN and the substrate have been proved to be leakage passages or photo-generated carrier deathnium centers or nonradiative recombination centers for GaN-based devices [13,14]. To suppress the undesirable influence of dislocations on the GaN-based UV-PDs and improve their performance, a great many investigations have been carried out, including dislocation filtering by self-assembled monolayer of silica microspheres [15], dislocation passivating by SiO_2 nanoparticles [16], dislocation filtering by selective area growth by a nanoporous template [17]. Recently, screw dislocation-driven self-assembled solution growth of one-dimensional (1D) semiconductor nanomaterials has offered a new opportunity to engineer and improve the performance of optoelectronic devices. It has been proved that, under low super-saturated solutions, the layer-by-layer growth was prohibited due to the energy penalty for creating a new surface layer and growth

* Corresponding author.
** Corresponding author.
E-mail addresses: zhengmeilin2011@126.com (C.H. Zheng), chenyr@ciomp.ac.cn (Y.R. Chen).

https://doi.org/10.1016/j.jallcom.2018.10.281
0925-8388/

occurred in a meritocratic way only at the axial screw dislocation spiral causing highly anisotropic 1D growth [18–21]. It can be a promising way to control the influence of screw dislocations on the performance of the GaN-based UV-PDs by self-driven *in-situ* growth of 1D semiconductor nanomaterials along the screw dislocations.

So far, 1D semiconductor nanomaterials such as nanowires (NWs), nanorods (NRs), and nanotubes (NTs) have been successfully assembled into a great many kinds of microelectronic and optoelectronic devices, including field effect transistors (FETs) [22–24], light-emitting diodes (LEDs) [25–28], nanolasers [29–31], photovoltaic cells [32–35], photodetectors (PDs) [36–38], and so on. Among them, in particular, zinc oxide (ZnO) has attracted a considerable attention because it is not only rich in nanostructures, but also belonging to a kind of direct wide bandgap semiconductor with a bandgap of 3.37 eV, which is very close to that of GaN (3.4 eV) [36]. Moreover, ZnO shares the same crystalline structure as GaN with a small lattice mismatch (both belonging to the wurtzite structure with $a_{ZnO} = 3.2498$ Å and $a_{GaN} = 3.1891$ Å) [39] that ensures a high-quality heterojunction can be achieved. More importantly, GaN epilayer prepared by the heteroepitaxy contains high densities of screw dislocations which have been proved to be acting as dislocation sources to propagate screw dislocation-driven 1D ZnO nanomaterials growth [19]. Therefore, taking advantage of the screw dislocations of the GaN epilayer, *in situ* self-driven growth of 1D ZnO nanomaterials can be developed into a new method to modify the defects viz. threading dislocations of the GaN-based semiconductor materials so as to achieve the purpose of regulating the performance of the GaN-based optoelectronic devices.

In this work, the back-illuminated metal-semiconductor-metal (MSM) structure UV-PDs based on p-GaN are modified by 1D ZnO nanorods using the screw dislocation-driven *in situ* growth method. The effects of 1D ZnO nanorods on the performance of GaN-based UV-PDs are also investigated in detail. The results show that the performance of the back-illuminated GaN-based UV-PDs can be greatly improved by modifying their screw dislocations with 1D ZnO nanorods. The *in-situ* self-assembled grown 1D ZnO nanorods play the role of passivating dislocations and constructing a series of nanoscale ZnO nanorods/p-GaN heterojunctions. This paper explores an approach, based on screw dislocation-driven *in-situ* self-assembled growth of 1D ZnO nanomaterials, to engineer and improve the GaN-based UV-PDs, which can be extended to other material systems of optoelectronic devices.

2. Experimental details

2.1. Preparation of p-GaN epilayer

The p-GaN epilayer was grown on a 2″ single polished c-plane sapphire substrate by low-pressure metal-organic chemical vapor deposition (LP-MOCVD). Trimethylgallium (TMGa) and ammonia (NH_3) were used as Ga and N precursors, respectively, while dicyclopentadienyl magnesium (Cp_2Mg) was used as the p-type dopant. Hydrogen (H_2) was used as the carrier gas. Prior to the growth, the sapphire substrate was thermally desorbed at 1100 °C under H_2 for 10 min. Then, an intrinsic GaN layer was grown on the sapphire substrate using a conventional two-step method, with a 30-nm-thick low-temperature GaN (LT-GaN) nucleation layer grown at 550 °C and a 2-μm-thick high-temperature GaN (HT-GaN) epilayer grown at 1050 °C. The intrinsic GaN was followed by a 1.5-μm-thick Mg-doped GaN (p-GaN) layer grown at 950 °C. The hole carrier concentration and the mobility of the p-GaN layer were measured to be $3.2 \times 10^{17}/cm^3$ and 6.8 $cm^2/(V \cdot s)$, respectively.

2.2. In-situ modification of 1D ZnO nanorods on a p-GaN layer

Prior to the screw dislocation-driven aqueous growth of 1D ZnO nanorods, the surface of the p-GaN film was firstly underwent degreasing treatment in isopropyl alcohol solution for 3 min, and then immersed into aqua regia for 8 min to remove the surface oxide layer. Subsequently, the surface of the p-GaN film was etched for 5 min with a boiling 10 wt% solution of potassium hydroxide solution. After rinsing by the deionized water, the growth of 1D ZnO nanorods was performed in a reaction kettle containing 20 mM $Zn(NO_3)_2$/hexamethylenetetramine (HMT) aqueous solution at 100 °C for 4 h.

2.3. Device fabrication

Before the device fabrication, in order to activate the Mg dopants in the p-GaN material, the p-GaN was rapidly annealed at 850 °C for 60 s under an N_2 atmosphere. In the subsequent process of fabricating the MSM structure photodetectors, Ni/Au (30 nm/200 nm) interdigital electrodes were deposited by electron-beam evaporation assisted by standard photolithography and lift-off processes. The dimensions of the finger electrodes were 100 μm long and 7 μm wide with a spacing of 8 μm. Finally, the photodetectors were annealed by rapid thermal annealing in an N_2 atmosphere at 450 °C for 120 s.

2.4. Characterization and measurement

The surface morphology of the p-GaN epilayer was characterized by an atomic force microscope (AFM, Veeco multi-mode). The carrier concentration and the mobility of the p-GaN epilayer were evaluated by Hall effect measurement system (Lake Shore, 8400 Series HMS). The cross-sectional image of the p-GaN epilayer and the morphologies of the MSM photodetectors with and without 1D ZnO nanorods were characterized by field-emission scanning electron microscope (SEM, Hitachi S4800). A high-resolution X-ray diffractometer (HRXRD, Bruker D8) with a Cu $K\alpha_1$ radiation ($\lambda = 1.5406$ Å) was used to evaluate the crystalline properties of the materials, mainly using the rocking curve scan, 2θ-ω scan and asymmetrical reciprocal space mapping (RSM) around the $(10\bar{1}5)$ reflection. The spectral responsivity and corresponding external quantum efficiency (EQE) for the photodetectors were measured using an ultraviolet spectral response test system. The PL spectra were measured by a spectrophotometer with a 50 mW 213-nm-wavelength Nd: YAG deep UV laser as the excitation source. The transient spectral response of the photodetectors was stimulated by a 10 mW 266-nm-wavelength Nd: YAG deep UV laser and recorded by a digital oscilloscope (Tektronix DPO 5104). A semiconductor parameter analyzer (Agilent B1500A) was used to measure the current-voltage (I-V) characteristics of the MSM structure photodetectors in dark and under the illumination of 367 nm light.

3. Results and discussion

Fig. 1(a) and (b) present the schematic illustrations of the *in-situ* modification of 1D ZnO nanorods on the screw dislocations that are contained within a p-GaN epilayer by screw dislocation-driven self-assembled aqueous solution growth method. In Fig. 1(c), the amplitude mode AFM image shows the top-down view of screw dislocations on the p-GaN epilayer. The scan area is $20 \times 20\ \mu m^2$. As can be seen, due to the lattice mismatch between the GaN and the sapphire substrate, it will form defects that become dislocation cores. During the step growth process of GaN, the newly generated step around the dislocation core will propagate at the same rate

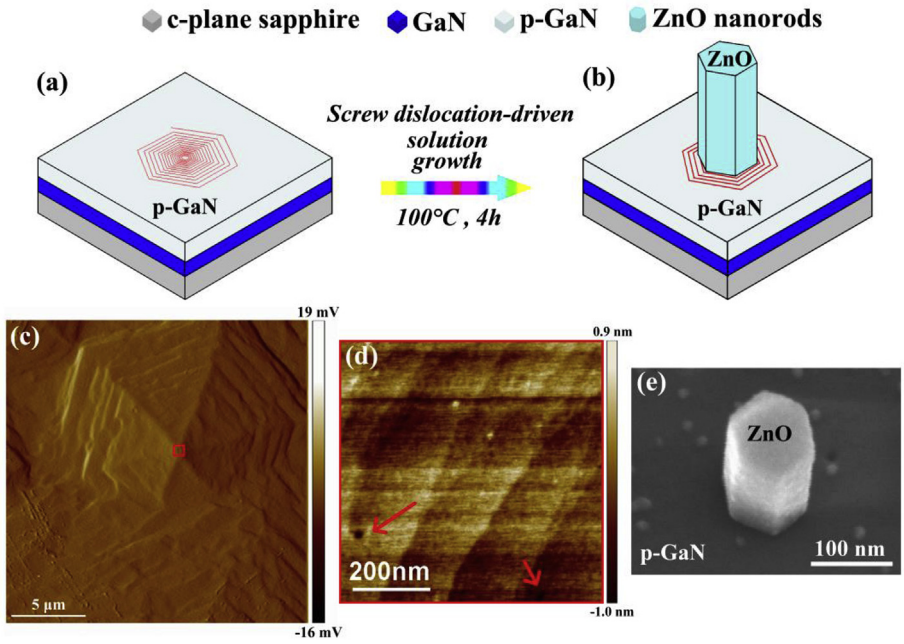

Fig. 1. Schematic of screw dislocation-driven solution growth of 1D ZnO nanorods on a p-GaN substrate. (a) Illustration of a screw dislocation exposed to the surface of the p-GaN. (b) Illustration of a screw dislocation-driven grown 1D ZnO nanorod by the method of solution growth. (c) The amplitude mode AFM image shows the top-down view of dislocations on the p-GaN layer. The scan area of AFM image is $20 \times 20\ \mu m^2$. (d) High magnification height mode AFM image of the area marked in (c). The locations pointed by the red arrows are on behalf of the screw dislocations. (e) The 30° tilted SEM image of a screw dislocation-driven solution grown 1D ZnO nanorod on a p-GaN layer. (For interpretation of the references to color in this figure legend, the reader is referred to the Web version of this article.)

with earlier steps at the outer edge of the growth spiral and thus forms a dislocation hillock with a step pile up [20]. The center of the dislocation hillock (marked by a red rectangle) is enlarged in the height mode of AFM, as shown in Fig. 1(d). The typical screw dislocations are just pointed by red arrows. According to the classical crystal growth theory, the supersaturation of the system is proposed to be the driving force for crystal growth in solutions [40]. Moreover, the dislocation-driven growth mode dominates the crystal growth under a low supersaturation condition. Herein, the screw dislocations usually create step edges upon intersection with a crystal surface to which atoms can be added without overcoming the energy barrier to nucleate new crystal steps [20,41]. Therefore, the crystal growth of 1D ZnO nanorods will propagate along the spiraled direction. Fig. 1(e) presents the 30° tilted SEM image of a screw dislocation-driven solution grown 1D ZnO nanorod on a p-GaN layer as a representative, which is prepared by the method described in the experimental section. As can be seen, the 1D ZnO nanorod has a whole hexagonal prism shape with an outer radius of about 100 nm and is perpendicular to the surface of p-GaN indicating its growth direction along the c-axis (the direction the screw dislocation spiraling upward). This process provides experimental conditions for the subsequent *in situ* solution growth of 1D ZnO nanorods on MSM structure p-GaN UV-PDs.

In order to study the influence of 1D ZnO nanorods on the optoelectric characteristics of the MSM structure p-GaN UV-PDs, the MSM structure p-GaN UV-PDs are prepared at first. The schematic illustration is shown in Fig. 2(a). In this process, MSM structure p-GaN UV-PDs are prepared as depicted in experimental section prior to the screw dislocation-driven solution growth of 1D ZnO nanorods. The SEM image of an as-fabricated MSM structure p-GaN UV-PD is shown in Fig. 2(b). Then, the as-fabricated device is placed in a reaction kettle with 20 mM $Zn(NO_3)_2$/hexamethylenetetramine (HMT) aqueous solution keeping at 100 °C for 4 h. The screw dislocation-driven *in-situ* self-assembled growth of 1D ZnO nanorods on the p-GaN between the interdigital electrode gaps will be completed in this process. Fig. 2(c) shows the SEM image of the MSM structure p-GaN UV-PD after solution growth of 1D ZnO nanorods. The partial enlarged SEM images (Fig. 2(d)-(f)) are provided as representatives to confirm the morphology and distribution of the 1D ZnO nanorods on the p-GaN between the interdigital electrode gaps.

To investigate the crystalline quality of the 1D ZnO nanorods/p-GaN heterostructure, XRD patterns are measured as shown in Fig. 3. For comparison, the (0002) plane 2θ-ω scan result of the as-grown p-GaN epilayer is firstly presented in Fig. 3(a), which has a single diffraction peak centered at 34.57° (pointed by a red arrow). In the (0002) plane 2θ-ω scan curve of Fig. 3(d), there is another diffraction peak located at 34.46° (pointed by a blue arrow) which is according to the (0002) diffraction peak of ZnO, in addition to the diffraction peak of p-GaN. The appearance of the ZnO (0002) peak indicates that the 1D ZnO nanorods are hexagonal structured and strict c-axis oriented, which is quite in line with the previous SEM result (as shown in Fig. 1(e)) and the direction the screw dislocation of the p-GaN epilayer spiraling upwards. Fig. 3(b) shows the asymmetrical RSM image around the $(10\bar{1}5)$ reflection for p-GaN, in which a well-resolved main peak surrounded by a series of contour lines distinguished by colors are presented. The axes of the RSM image are stood for the directions parallel and perpendicular to the surface of the p-GaN epilayer, and the reciprocal lattice point (RLP) (q_x, q_z) can be used to calculate the in-plane and out-plane lattice constants via the following relations [12,42].

$$a = 2\left[\left(h^2 + hk + k^2\right) \Big/ \left(3q_x^2\right)\right]^{1/2} \quad (1)$$

$$c = l/q_z \quad (2)$$

where h, k, and l are the Miller indices. The lattice constants for fully relaxed bulk GaN are 0.31891 nm and 0.51855 nm for a_0 and c_0, respectively [43]. Thus, the RLP denoted as (q_{x0}, q_{z0}) for fully

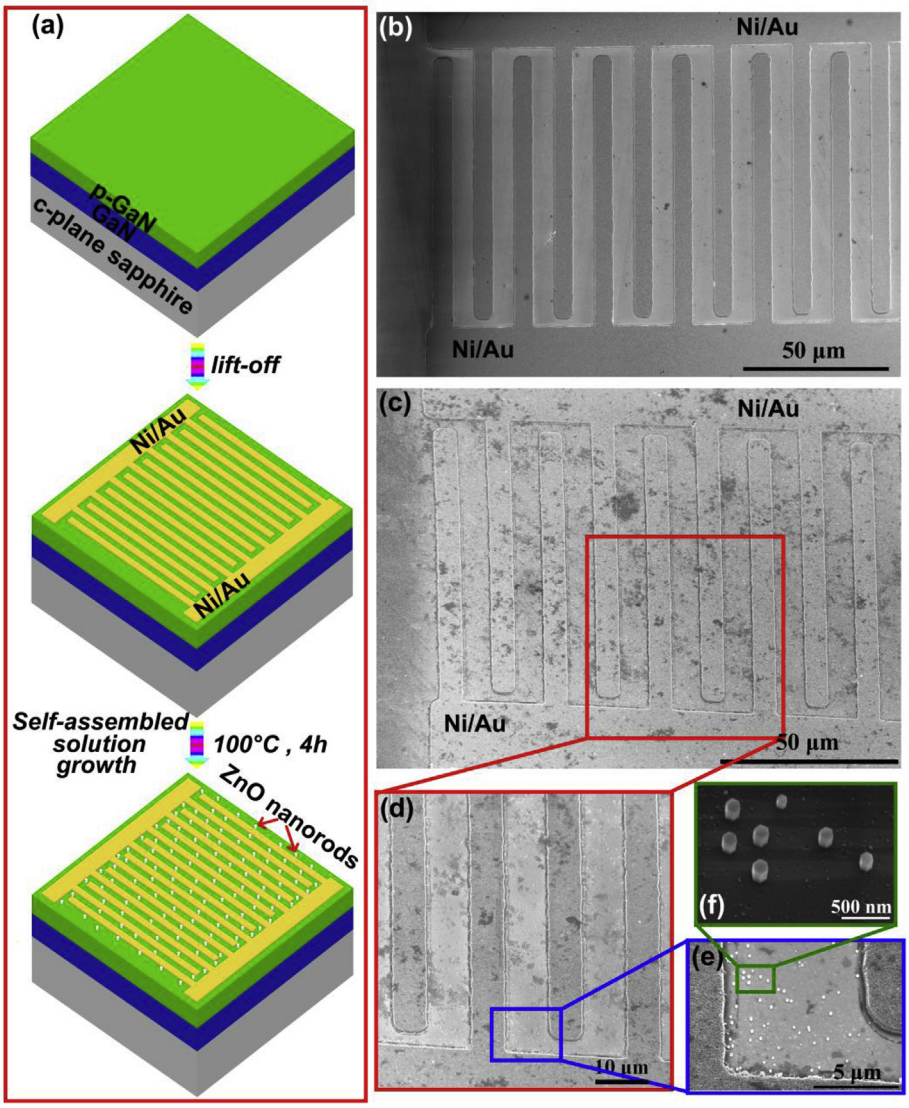

Fig. 2. (a) Schematic illustration of the fabrication of 1D ZnO nanorods on the MSM structure p-GaN photodetector. (b) The SEM image of the as-fabricated MSM structure p-GaN photodetector. (c) The SEM image of the MSM structure p-GaN photodetector after solution growth of 1D ZnO nanorods on p-GaN. (d), (e) and (f) The partial enlarged SEM images to confirm the self-assembled heterogeneous growth of 1D ZnO nanorods on the p-GaN between the interdigital electrode gaps.

relaxed GaN, can be calculated as (−3.621, 9.642) for its $(10\bar{1}5)$ reflection. In Fig. 3(b), the RLP denoted as (q_x, q_z) for the main peak of p-GaN is measured as (−3.62, 9.642) for the $(10\bar{1}5)$ reflection, which means that the p-GaN epilayer is almost unstrained. In order to evaluate the strain evolution in the screw dislocation-driven growth of 1D ZnO nanorods on p-GaN, the asymmetrical RSM image around the $(10\bar{1}5)$ reflection for the ZnO nanorods/p-GaN heterostructure is also demonstrated, as shown in Fig. 3(e). In contrast with Fig. 3(b), there are two well-resolved main peaks in Fig. 3(e). The one denoted as (−3.62, 9.642) is corresponding to the main peak of the p-GaN which is the same as that of the as-grown one. This means that the introduction of 1D ZnO nanorods by the method of screw dislocation-driven self-assembled aqueous solution growth has little impact on the strain state of p-GaN. The red cross-point is on behalf of the RLP for the main peak of the 1D ZnO nanorods, which is measured as (−3.545, 9.61). Referring to the lattice constants of unstrained hexagonal ZnO nanomaterials ($a_0 = 0.32498$ nm and $c_0 = 0.52066$ nm) [44], the RLP denoted as (q_{x0}, q_{z0}) for unstrained 1D ZnO nanorods can be calculated as (−3.553, 9.603) for its $(10\bar{1}5)$ reflection. It is found that the q_x of ZnO nanorods grown on the dislocations of p-GaN decreases while the q_z increases. In real space, it reveals dilatation of in-plane lattice constant a and shrinkage of out-plane lattice constant c. The related strains $\varepsilon_{xx} \sim \left(\frac{1}{q_x} - \frac{1}{q_{x0}}\right) \times q_{x0}$ and $\varepsilon_{zz} \sim \left(\frac{1}{q_z} - \frac{1}{q_{z0}}\right) \times q_{z0}$ can be calculated to be 0.225% and −0.073%, respectively, which discloses that the 1D ZnO nanorods grown on the dislocations of p-GaN epilayer by *in-situ* self-assembled solution growth method are subjected to tensile strain and compressive strain respectively in the directions parallel to and perpendicular to the surface of p-GaN, due to the lattice mismatch between the ZnO and p-GaN. Fig. 3(c) and (f) present the (0002) plane rocking curves for p-GaN and 1D ZnO nanorods, and the full width at half-maximum (FWHM) can be evaluated to be 0.07° and 0.156°, respectively.

The room-temperature PL spectra of the as-grown p-GaN, 1D ZnO nanorods, and 1D ZnO nanorods/p-GaN heterostructure are also measured and analyzed in Fig. 4. In comparison, the spectrum of the p-GaN layer (Fig. 4(a)) shows a single emission peak at

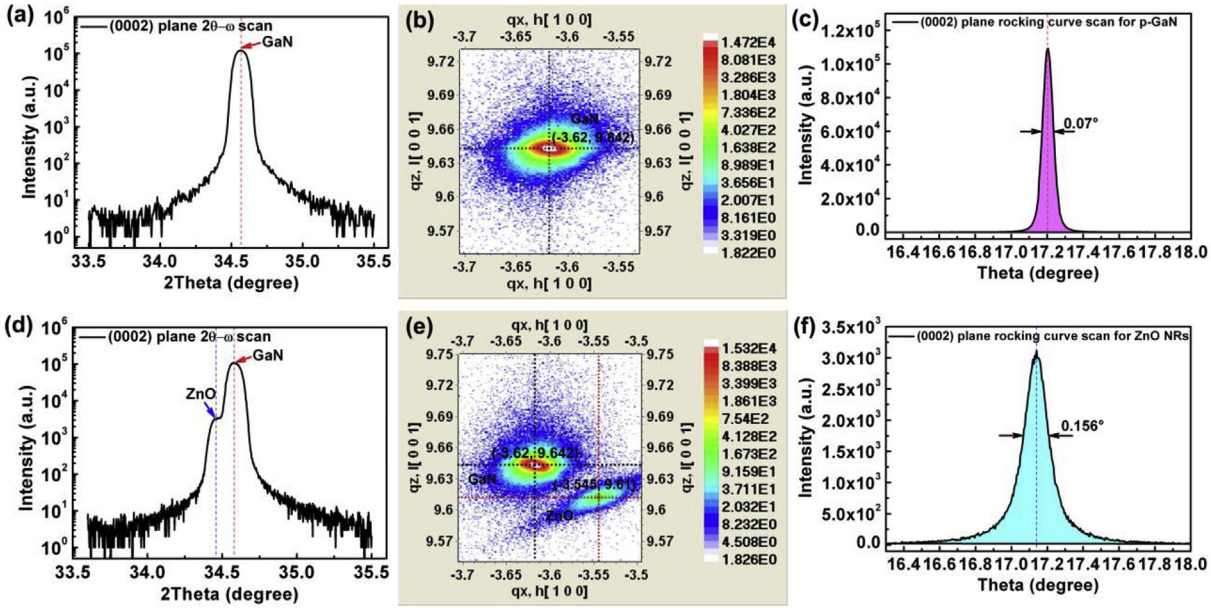

Fig. 3. XRD patterns for the p-GaN epilayer and the ZnO nanorods/p-GaN heterostructure. (a) 2θ-ω scan result from the (0002) plane for p-GaN epilayer. (b) The asymmetrical RSM around the $(10\bar{1}5)$ reflection for p-GaN. (c) The (0002) plane rocking curve for p-GaN. (d) 2θ-ω scan result from the (0002) plane for the ZnO nanorods/p-GaN heterostructure. (e) The asymmetrical RSM around the $(10\bar{1}5)$ reflection for the ZnO nanorods/p-GaN heterostructure. (f) The (0002) plane rocking curve for 1D ZnO nanorods.

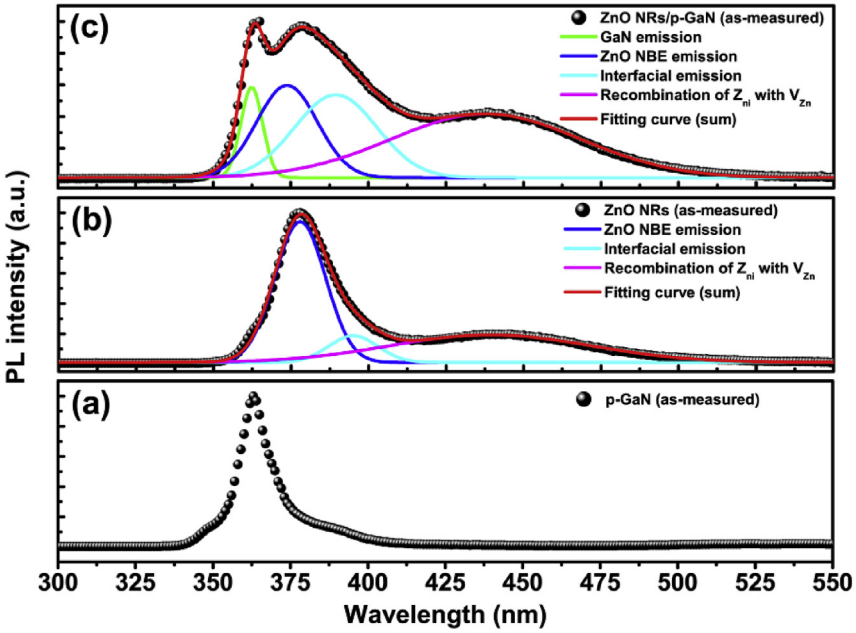

Fig. 4. PL spectra of (a) p-GaN, (b) 1D ZnO nanorods, and (c) 1D ZnO nanorods/p-GaN heterostructure.

363 nm with a FWHM of 12 nm, which is attributed to the intrinsic luminescence of p-GaN and strictly in accordance with the band gap of GaN (3.41 eV). No blue emission due to a transition between the conduction band and the deep Mg dopant levels is observed for the epilayer. The as-measured spectrum of the 1D ZnO nanorods is shows in Fig. 4(b) using black scatters. A well multi-peaks Gaussian fitting gives three Gaussian bands centering at ~377 nm, ~395 nm, and ~439 nm. Among them, the peak located at ~377 nm is corresponding to the intense near-band-edge (NBE) emission of ZnO which is attributed to the free-exciton emission of ZnO. The peak centered at ~395 nm can be ascribed to the interfacial emission of the ZnO nanorods/p-GaN heterojunction. Due to the interference from the heterogeneous interface during the *in-situ* measurement, a weak interfacial emission peak is observed in the PL spectrum of 1D ZnO nanorods. In addition, a broad peak on the long wavelength side centered at 439 nm is proved to be the recombination of the interstitial zinc (Zn_i) with zinc vacancies (V_{Zn}) [45,46]. The PL spectrum of 1D ZnO nanorods is different from that of ZnO nanorods containing screw dislocations reported by Dai et al. [47], which indicates that the 1D ZnO nanorods prepared in our work are almost free of screw dislocations. For the PL spectrum of the 1D ZnO nanorods/p-GaN heterostructure, as shown in Fig. 4(c), a well multi-peaks Gaussian fitting confirms the material structure with four dominant emission peaks in accordance with those of p-GaN and 1D ZnO nanorods.

The spectral responsivities for the MSM structure p-GaN

photodetector with and without 1D ZnO nanorods under different bias voltage are measured to demonstrate the role of the 1D ZnO nanorods, as shown in Fig. 5. During the measurement, both of the as-fabricated photodetector and 1D ZnO nanorods modified one are back-illuminated by the incident light. Their response spectra present a bandpass characteristic, as shown in Fig. 5(a) and (b). The response spectrum of the MSM structure p-GaN photodetector without 1D ZnO nanorods ranges from 362 nm to 375 nm with a peak value of 0.085 A/W at 367 nm under 1 V bias voltage, corresponding to an external quantum efficiency (EQE) of 28.7%, which increases to 0.103 A/W at 3 V with an EQE of 34.6%. By comparison, the response spectra of the MSM structure p-GaN photodetector with 1D ZnO nanorods present an extended range between 362 nm and 385 nm with peak values of 0.118 A/W and 0.147 A/W at 368 nm under 1 V and 3 V bias voltages, corresponding to EQEs of 39.9% and 49.6%, respectively. Viz., the modification of the dislocations of p-GaN using 1D ZnO nanorods not only improves the spectral response intensity of the MSM structure p-GaN photodetector but also extends its bandpass wavelength width. The mechanism involved can be clarified by the energy band diagram shown in Fig. 5(c). Referring to Fig. 2(d)-(f), on the surface of the p-GaN between the interdigital electrode gaps, there distributes a large number of isolate 1D ZnO nanorods grown upon the dislocations of the p-GaN. Each one of the 1D ZnO nanorods will form a nanoscale heterojunction with p-GaN. Under the thermal equilibrium condition, each heterogeneous interface of the ZnO nanorod/p-GaN will form a localized depletion region and generates a built-in electric field (E) directed from ZnO nanorod to p-GaN, which is conducive to the separation of the photo-generated electron-hole pairs in the depletion region. It should be noted that in general, the depletion width of the p-GaN side is greater than that of ZnO side due to its lower carrier concentration. Furthermore, in the back-illuminated MSM structure ZnO nanorods/p-GaN photodetector, the incident light illuminated from the sapphire side is firstly absorbed by the p-GaN layer, exciting electron-hole pairs which separate and transport to the interdigital electrodes under the applied bias. Only the light with wavelength longer than 363 nm can pass through the p-GaN layer and reach the 1D ZnO nanorods. Therefore, a considerable additional photo-generated electron-hole pairs will be produced in a series of depletion regions and 1D ZnO nanorods. The representative carrier diffusion process is shown in the energy band model in which the electron affinities (χ) for GaN and ZnO are 4.2 eV and 4.35 eV while their bandgap values (E_g) at room temperature are 3.41 eV and 3.37 eV, respectively [48]. For a close contacted ZnO nanorod/p-GaN heterojunction, the band offsets are calculated as 0.15 eV between the two conduction bands (ΔE_c) and 0.11 eV between the two valence bands (ΔE_v). Owning to the small band offsets, the considerable additional photo-generated electron-hole pairs generated in the depletion regions and 1D ZnO nanorods will separate and pass through the barrier under the built-in electric field (E) and drift to the interdigital electrodes as a contribution to the photocurrent under the applied bias of the MSM photodetector. Therefore, the enhancement of the spectral response intensity as well as the extension of the spectral response range in the ZnO nanorods/p-GaN MSM structure photodetector originate from the photoelectric response in a series of nanoscale heterojunctions and 1D ZnO nanorods. Indeed, compared Fig. 5(a) with Fig. 4, the cut-off wavelength of the spectral response for the back-illuminated ZnO nanorods/p-GaN MSM structure photodetector is almost according with the main peaks of its PL spectrum.

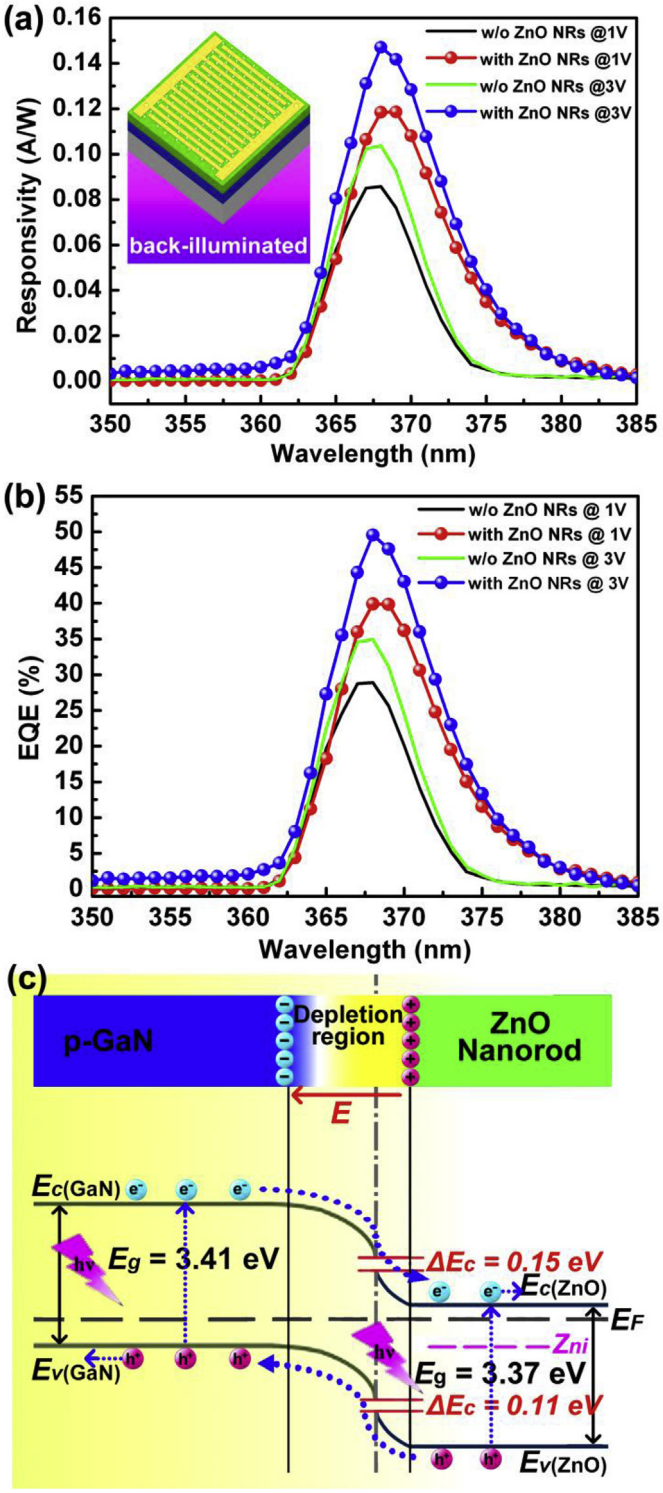

Fig. 5. Spectral characteristics for the MSM structure p-GaN photodetector with and without 1D ZnO nanorods under different bias voltage. (a) The responsivities and (b) the corresponding EQEs. (c) The energy band diagram of ZnO nanorods/p-GaN heterostructure at zero-bias voltage.

In Fig. 6(a), it shows the current-voltage (I-V) characteristics of the MSM structure p-GaN photodetector with and without 1D ZnO nanorods in dark and under the 367-nm-wavelength illumination using a semi-logarithmic scale. As can be seen, the dark current of the MSM structure p-GaN photodetector with 1D ZnO nanorods is slightly lower than that of the as-fabricated one, which can be attributed to the dislocations passivating by *in-situ* grown 1D ZnO nanorods. In addition, the photocurrent of the photodetector modified with 1D ZnO nanorods is also greatly enhanced about one order of magnitude in comparison with that of the as-fabricated one under a certain wavelength of the incident light. This result

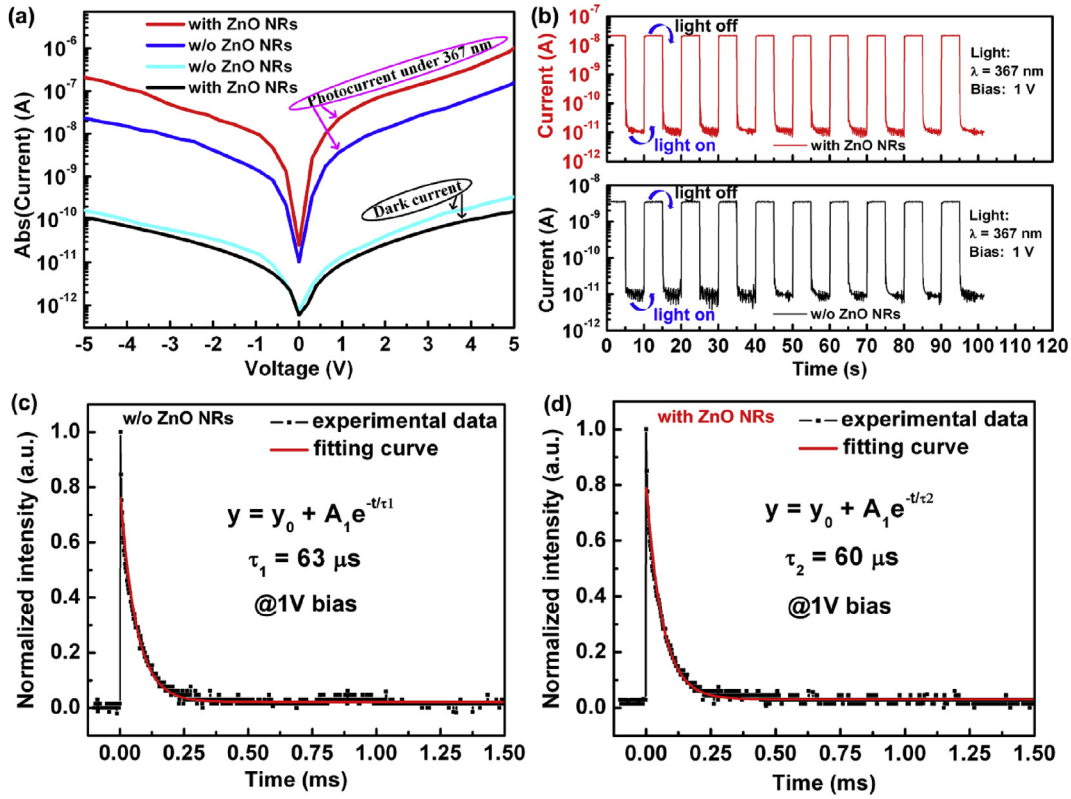

Fig. 6. (a) The I-V characteristics of the MSM structure p-GaN photodetector with and without 1D ZnO nanorods in dark and under the illumination of 367 nm light using the semi-logarithmic scale. (b) Time-dependent photocurrent response of the MSM structure p-GaN photodetector with and without 1D ZnO nanorods under the conditions of 367-nm-wavelength illumination and 1 V bias. (c) Decay edge of the transient spectral response under 1 V bias for the photodetector without 1D ZnO nanorods and (d) with 1D ZnO nanorods.

strongly reflects the photoelectric enhancement effect of the 1D ZnO nanorods. Fig. 6(b) shows the time-dependent photocurrent responses of the MSM structure p-GaN photodetector with and without 1D ZnO nanorods under the conditions of 367-nm-wavelength illumination and 1 V bias. Both exhibit rapid and stable response to the 367-nm-wavelength light when it is on or off. The corresponding decay edges of the transient spectral response under 1 V bias are demonstrated in Fig. 6(c) and (d), respectively. Both decay sections are well fitted by a first-order exponential decay function with a decay component of about 63 μs (τ_1) for the p-GaN photodetector without 1D ZnO nanorods and 60 μs (τ_2) for that with 1D ZnO nanorods. The slight improvement of the decay time in the ZnO nanorods/p-GaN MSM structure photodetector can be ascribed to the presence of a series of localized built-in electric fields located at the interface of the nanoscale heterojunctions that is good for the separation and transport of the photo-generated carriers so as to decrease the instantaneous equivalent capacitance of the device, and thus reducing its RC constant.

4. Conclusions

In summary, we have demonstrated the *in-situ* self-assembled aqueous solution growth of 1D ZnO nanorods on a p-GaN epilayer by a screw dislocation-driven method and deliberately modified the screw dislocations in the p-GaN MSM structure ultroviolet photodetector with 1D ZnO nanorods for the purpose of engineering and improving its photoelectric performances. The role of the 1D ZnO nanorods in the back-illuminated p-GaN MSM structure photodetector has been investigated in detail. The results show that due to the introduction of 1D ZnO nanorods on the dislocations of the p-GaN epilayer, the dark current of the MSM structure ZnO nanorods/p-GaN photodetector is suppressed to some extent, which can be attributed to the passivating role of the *in-situ* grown 1D ZnO nanorods on the dislocations in the p-GaN layer. Moreover, the presence of 1D ZnO nanorods on the p-GaN MSM structure photodetector not only improves its spectral response intensity but also extends its spectral response band. Meanwhile, the decay time of the transient spectral response is also improved. The phenomenon involved can be originated from the photoelectric response in a series of nanoscale heterojunctions and 1D ZnO nanorods. A considerable additional photo-generated electron-hole pairs generated in the depletion regions and 1D ZnO nanorods will separate and pass through the barrier under the built-in electric field of the heterojunction and drift to the inter-digital electrodes as a contribution to the photocurrent under the applied bias of the MSM photodetector. Based on the screw dislocation-driven self-assembled growth of 1D ZnO nanomaterials for modification, it is an approach to engineer and improve the GaN-based UV-PDs, which can be extended to other material systems of optoelectronic devices.

Acknowledgements

This work is partially supported by the Natural Science Foundation of Fujian Province of China (Grant No. 2017J01713), the National Natural Science Foundation of China (Grant Nos. 61504144 and 51472230), the Science and Technology Bureau Project of Quanzhou City of China (Grant No. 2014Z118), and the Jilin Provincial Science & Technology Department (Grant No. 20170520156JH).

References

[1] L.X. Su, Q.L. Zhang, T.Z. Wu, M.M. Chen, Y.Q. Su, Y. Zhu, R. Xiang, X.C. Gui, Z.K. Tang, High-performance zero-Bias ultraviolet photodetector based on p-GaN/n-ZnO heterojunction, Appl. Phys. Lett. 105 (2014), 072106.

[2] S.I. Inamdar, K.Y. Rajpure, High-performance metal-semiconductor-metal UV photodetector based on spray deposited ZnO thin films, J. Alloys Compd. 595 (2014) 55–59.

[3] S. Park, S. Kim, G.J. Sun, D.B. Byeon, S.K. Hyun, W.I. Lee, C. Lee, ZnO-core/ZnSe-shell nanowires UV photodetector, J. Alloys Compd. 658 (2016) 459–464.

[4] E. Matioli, S. Brinkley, K.M. Kelchner, Y.-L. Hu, S. Nakamura, S. DenBaars, J. Speck, C. Weisbuch, High-brightness polarized light-emitting diodes, Light Sci. Appl. 1 (2012) e22.

[5] Y.H. Lin, S.Z. Zhou, W.L. Wang, W.J. Yang, H.R. Qian, H.Y. Wang, Z.T. Lin, Z.L. Liu, Y.N. Zhu, G.Q. Li, Performance improvement of GaN-based light-emitting diodes grown on Si(111) substrates by controlling the reactor pressure for the GaN nucleation layer growth, J. Mater. Chem. C 3 (2015) 1484–1490.

[6] D.Y. Kim, J.H. Park, J.W. Lee, S. Hwang, S.J. Oh, J. Kim, C. Sone, E.F. Schubert, J.K. Kim, Overcoming the fundamental light-extraction efficiency limitations of deep ultraviolet light-emitting diodes by utilizing transverse-magnetic-dominant emission, Light Sci. Appl. 4 (2015) e263.

[7] S.-H. Lim, Y.-H. Ko, C. Rodriguez, S.-H. Gong, Y.-H. Cho, Electrically driven, phosphor-free, white light-emitting diodes using gallium nitride-based double concentric truncated pyramid structures, Light Sci. Appl. 5 (2016), e16030.

[8] K.H. Li, X. Liu, Q. Wang, S. Zhao, Z. Mi, Ultralow-threshold electrically injected AlGaN nanowires ultraviolet lasers on Si operating at low temperature, Nat. Nanotechnol. 10 (2015) 140–144.

[9] N.V. Trivino, R. Butte, J.-F. Carlin, N. Grandjean, Continuous wave blue lasing in III-nitride nanobeam cavity on silicon, Nano Lett. 15 (2015) 1259–1263.

[10] A.G. Baca, A.M. Armstrong, A.A. Allerman, E.A. Douglas, C.A. Sanchez, M.P. King, M.E. Coltrin, T.R. Fortune, R.J. Kaplar, An AlN/$Al_{0.85}Ga_{0.15}N$ high electron mobility transistor, Appl. Phys. Lett. 109 (2016), 033509.

[11] G. Greco, F. Fiorenza, F. Iucolano, A. Severino, F. Giannazzo, F. Roccaforte, Conduction mechanisms at interface of AlN/SiN dielectric stacks with AlGaN/GaN heterostructures for normally-off high electron mobility transistors: correlating device behavior with nanoscale interfaces properties, ACS Appl. Mater. Interfaces 9 (2017) 35383–35390.

[12] Y.R. Chen, Z.W. Zhang, H. Jiang, Z.M. Li, G.Q. Miao, H. Song, The optimized growth of AlN templates for back-illuminated AlGaN-based solar-blind ultraviolet photodetectors by MOCVD, J. Mater. Chem. C 6 (2018) 4936–4942.

[13] M. Tapajna, S.W. Kaun, M.H. Wong, F. Gao, T. Palacios, U.K. Mishra, J.S. Speck, M. Kuball, Influence of threading dislocation density on early degradation in AlGaN/GaN high electron mobility transistors, Appl. Phys. Lett. 99 (2011), 223501.

[14] A. Armstrong, T.A. Henry, D.D. Koleske, M.H. Crawford, K.R. Westlake, S.R. Lee, Dependence of radiative efficiency and deep level defect incorporation on threading dislocation density for InGaN/GaN light emitting diodes, Appl. Phys. Lett. 101 (2012), 162102.

[15] Q.M. Li, J.J. Figiel, G.T. Wang, Dislocation density reduction in GaN by dislocation filtering through a self-assembled monolayer of silica microspheres, Appl. Phys. Lett. 94 (2009), 231105.

[16] X.J. Sun, D.B. Li, H. Jiang, Z.M. Li, H. Song, Y.R. Chen, G.Q. Miao, Improved performance of GaN metal-semiconductor-metal ultraviolet detectors by depositing SiO_2 nanoparticles on a GaN surface, Appl. Phys. Lett. 98 (2011), 121117.

[17] R. Colby, Z.W. Liang, I.H. Wildeson, D.A. Ewoldt, T.D. Sands, R.E. Garcia, E.A. Stach, Dislocation filtering in GaN nanostructures, Nano Lett. 10 (2010) 1568–1573.

[18] S.A. Morin, M.J. Bierman, J. Tong, S. Jin, Mechanism and kinetics of spontaneous nanotubes growth driven by screw dislocations, Science 328 (2010) 476–480.

[19] S.A. Morin, S. Jin, Screw dislocation-driven epitaxial solution growth of ZnO nanowires seeded by dislocations in GaN substrates, Nano Lett. 10 (2010) 3459–3463.

[20] F. Meng, S.A. Morin, A. Forticaux, S. Jin, Screw dislocation driven growth of nanomaterials, Accounts Chem. Res. 46 (2013) 1616–1626.

[21] A. Forticaux, S. Hacialioglu, J.P. DeGrave, R. Dziedzic, S. Jin, Three-dimensional mesoscale heterostructures of ZnO nanowires arrays epitaxially grown on $CuGaO_2$ nanoplates as individual diodes, ACS Nano 7 (2013) 8224–8232.

[22] S.K. Jha, C.P. Liu, Z.H. Chen, K.J. Chen, I. Bello, J.A. Zapien, W.J. Zhang, S.-T. Lee, Integrated nanorods and heterostructure field effect transistors for gas sensing, J. Phys. Chem. C 114 (2010) 7999–8004.

[23] R. Levi, O. Bitton, G. Leitus, R. Tenne, E. Joselevich, Field-effect transistors based on WS_2 nanotubes with high current-carrying capacity, Nano Lett. 13 (2013) 3736–3741.

[24] M. Shaygan, K. Davami, N. Kheirabi, C.K. Baek, G. Cuniberti, M. Meyyappan, J.-S. Lee, Single-crystalline CdTe nanowires field effect transistors as nanowires-based photodetector, Phys. Chem. Chem. Phys. 16 (2014) 22687–22693.

[25] O. Lupan, T. Pauporté, B. Viana, I.M. Tiginyanu, V.V. Ursaki, R. Cortès, Epitaxial electrodeposition of ZnO nanowires arrays on p-GaN for efficient UV-light-emitting diode fabrication, ACS Appl. Mater. Interfaces 2 (2010) 2083–2090.

[26] M. Tchernycheva, P. Lavenus, H. Zhang, A.V. Babichev, G. Jacopin, M. Shahmohammadi, F.H. Julien, R. Ciechonski, G. Vescovi, O. Kryliouk, InGaN/GaN core-shell single nanowire light emitting diodes with graphene-based p-contact, Nano Lett. 14 (2014) 2456–2465.

[27] X.B. Tang, G.M. Li, S.M. Zhou, Ultraviolet electroluminescence of light-emitting diodes based on single n-ZnO/p-AlGaN heterojunction nanowires, Nano Lett. 13 (2013) 5046–5050.

[28] H. Zhou, P.B. Gui, Q.H. Yu, J. Mei, H. Wang, G.J. Fang, Self-powered, visible-blind ultraviolet photodetector based on n-ZnO nanorods/i-MgO/p-GaN structure light-emitting diodes, J. Mater. Chem. C 3 (2015) 990–994.

[29] J.-Y. Zhang, Q.-F. Zhang, T.-S. Deng, J.-L. Wu, Electrically driven ultraviolet lasing behavior from phosphorus-doped p-ZnO nanonail array/n-Si heterojunction, Appl. Phys. Lett. 95 (2009), 211107.

[30] H.W. Xu, J.B. Wright, A. Hurtado, Q.M. Li, T.-S. Luk, J.J. Figiel, J. Cross, G. Balakrishnan, L.F. Lester, I. Brener, G.T. Wang, Gold substrate-induced single-mode lasing of GaN nanowires, Appl. Phys. Lett. 101 (2012), 221114.

[31] Y.P. Fu, H.M. Zhu, C.C. Stoumpos, Q. Ding, J. Wang, M.G. Kanatzidis, X.Y. Zhu, S. Jin, Broad wavelength tunable robust lasing from single-crystal nanowires of cesium lead halide perovskites ($CsPbX_3$, X = Cl, Br, I), ACS Nano 10 (2016) 7963–7972.

[32] Z.Y. Yin, S.X. Wu, X.Z. Zhou, X. Huang, Q.C. Zhang, F. Boey, H. Zhang, Electrochemical deposition of ZnO nanorods on transparent reduced graphene oxide electrodes for hybrid solar cells, Small 6 (2010) 307–312.

[33] B.Z. Tian, X.L. Zheng, T.J. Kempa, Y. Fang, N.F. Yu, G.H. Yu, J.L. Huang, C.M. Lieber, Coaxial silicon nanowires as solar cells and nanoelectronic power sources, Nature 449 (2007) 885–889.

[34] W. Wei, X.-Y. Bao, C. Soci, Y. Ding, Z.-L. Wang, D. Wang, Direct heteroepitaxy of vertical InAs nanowires on Si substrates for broad band photovoltaics and photodetection, Nano Lett. 9 (2009) 2926–2934.

[35] D.-Y. Son, J.-H. Im, H.-S. Kim, N.-G. Park, 11% efficient perovskite solar cell based on ZnO nanorods: an effective charge collection system, J. Phys. Chem. C 118 (2014) 16567–16573.

[36] H. Zhu, C.X. Shan, B. Yao, B.H. Li, J.Y. Zhang, D.X. Zhao, D.Z. Shen, X.W. Fan, High spectrum selectivity ultraviolet photodetector fabricated from an n-ZnO/p-GaN heterojunction, J. Phys. Chem. C 112 (2008) 20546–20548.

[37] V.Q. Dang, T.Q. Trung, D.-I. Kim, L.T. Duy, B.-U. Hwang, D.-W. Lee, B.-Y. Kim, L.D. Toan, N.-E. Lee, Ultrahigh responsivity in graphene-ZnO nanorod hybrid UV photodetector, Small 11 (2015) 3054–3065.

[38] A. Echresh, C.O. Chey, M.Z. Shoushtari, V. Khranovskyy, O. Nur, M. Willander, UV photo-detector based on p-NiO thin film/n-ZnO nanorods heterojunction prepared by a simple process, J. Alloys Compd. 632 (2015) 165–171.

[39] R.D. Vispute, V. Talyansky, S. Choopun, R.P. Sharma, T. Venkatesan, Heteroepitaxy of ZnO on GaN and its implications for fabrication of hybrid optoelectronic devices, Appl. Phys. Lett. 73 (1998) 348–350.

[40] I.V. Markov, Crystal Growth for Beginners: Fundamentals of Nucleation, Crystal Growth, and Epitaxy, World Scientific Publishing, Singapore, 1995.

[41] W.K. Burton, N. Cabrera, F.C. Frank, Role of dislocations in crystal growth, Nature 163 (1949) 398–399.

[42] A. Kadir, C.C. Huang, K.E.K. Lee, E.A. Fitzgerald, S.J. Chua, Determination of alloy composition and strain in multiple AlGaN buffer layers in GaN/Si system, Appl. Phys. Lett. 105 (2014), 232113.

[43] M. Yamaguchi, T. Yagi, T. Sota, T. Deguchi, K. Shimada, S. Nakamura, Brillouin scattering study of bulk GaN, J. Appl. Phys. 85 (1999) 8502–8504.

[44] Z.W. Pan, Z.R. Dai, Z.L. Wang, Nanobelts of semiconducting oxides, Science 291 (2001) 1947–1949.

[45] H. Zeng, G. Duan, Y. Li, S. Yang, X. Xu, W. Cai, Blue luminescence of ZnO nanoparticles based on non-equilibrium processes: defect origins and emission controls, Adv. Funct. Mater. 20 (2010) 561–572.

[46] C. Park, J. Lee, W.S. Chang, Geometrical separation of defect states in ZnO nanorods and their morphology-dependent correlation between photoluminescence and photoconductivity, J. Phys. Chem. C 119 (2015) 16984–16990.

[47] J. Dai, J. Lu, F. Wang, J. Guo, N. Gu, C. Xu, Optical and exciton dynamical properties of a screw-dislocation-driven ZnO: Sn microstructure, ACS Appl. Mater. Interfaces 7 (2015) 12655–12662.

[48] O. Lupan, T. Pauporté, B. Viana, Low-voltage UV-electroluminescence from ZnO-nanowire array/p-GaN light-emitting diodes, Adv. Mater. 22 (2010) 3298–3302.